VIP Electrocatalysis Very Important Paper

International Edition: DOI: 10.1002/anie.201915663
German Edition: DOI: 10.1002/ange.201915663

Transition-Metal–Boron Intermetallics with Strong Interatomic d–sp Orbital Hybridization for High-Performance Electrocatalysis

*Xuan Ai[+], Xu Zou[+], Hui Chen[+], Yutong Su, Xilan Feng, Qiuju Li, Yipu Liu, Yu Zhang, and Xiaoxin Zou**

Abstract: *A theoretical and experimental study gives insights into the nature of the metal–boron electronic interaction in boron-bearing intermetallics and its effects on surface hydrogen adsorption and hydrogen-evolving catalytic activity. Strong hybridization between the d orbitals of transition metal (T_M) and the sp orbitals of boron exists in a family of fifteen T_M–boron intermatallics (T_M:B = 1:1), and hydrogen atoms adsorb more weakly to the metal-terminated intermetallic surfaces than to the corresponding pure metal surfaces. This modulation of electronic structure makes several intermetallics (e.g., PdB, RuB, ReB) prospective, efficient hydrogen-evolving materials with catalytic activity close to Pt. A general reaction pathway towards the synthesis of such T_MB intermetallics is provided; a class of seven phase-pure T_MB intermetallics, containing V, Nb, Ta, Cr, Mo, W, and Ru, are thus synthesized. RuB is a high-performing, non-platinum electrocatalyst for the hydrogen evolution reaction.*

The surface chemisorption properties of heterogeneous catalysts play crucial roles in their catalytic activity, stability, and selectivity. The correlation between surface chemisorption properties and catalytic behaviors has been empirically summarized as Sabatier principle.[1] In general, the key reaction intermediates should bind neither too strongly nor too weakly on the desirable catalyst surface, as classically shown for transition-metal-based catalysts. This knowledge has had great guiding significance in catalyst design.[1,2] One of the goals in current catalysis research is to optimize the surface chemisorption and thereby catalytic properties of catalysts by tuning the local atomic structures of active sites. To this end, multi-element alloying is an effective way to adjust the local coordination environment of the active sites for achieving the optimization of surface chemisorption and thus the improvement of catalytic properties.[3] This mainly because each alloy, especially intermetallic compounds, generally has specific electronic and crystal structures that are different from its constituent elements, and thus possesses unique surface adsorption and catalytic abilities. This intrinsic feature, together with the variety and richness of intermetallics,[4] makes this family of materials a striking addition to heterogeneous catalysts.

With the progress of computational chemistry and synthetic inorganic chemistry, a number of transition-metal-containing intermetallics are explored both theoretically and experimentally for a range of important reactions, such as the HER, the oxygen reduction reaction (ORR), and so on.[1–4] For example, the d-band model has been established by Nørskov et al. to explain and predict the chemisorption and catalytic properties of transition-metal-containing intermetallics,[1,5] and to rationalize the relevant experimental results.[6] On the other hand, some experimental methods have been reported to synthesize various intermetallics with designable electronic/geometric structures and advanced catalytic performances.[3,6,7] Although many progresses regarding the intermetallic catalysts have been made, the majority of relevant researches focus on the intermetallics containing a combination of multiple metals.[1,4] Additionally, despite their large number, structural diversity, and impressive physical properties (for example, superconductivity),[8] the intermetallics with a combination of one or more metals with boron are less studied for catalysis applications. The reasons behind this situation mainly lie in two aspects: 1) the lack of enough knowledge about the roles of metal–boron electronic interactions in surface chemisorption and catalysis; and 2) the lack of enough boron-bearing intermetallics that are available for catalysis studies because of the difficult synthesis of catalysis-applicable, phase-pure samples.[9]

Herein, we report a combined theoretical and experimental study to demonstrate the important role of metal–boron electronic interactions in surface hydrogen chemisorption and catalytic activity for the HER. Our theoretical results show the atomic hydrogen adsorption to the metal-terminated intermetallic surfaces is weaker than to the corresponding pure metal surfaces. This is due to the modified d-band properties governed by the strong hybridization between d orbitals of the transition metal and the sp orbitals of boron. Our theoretical results also predict several T_MB intermetallics (PdB, RuB, ReB) as highly active hydrogen-evolving catalysts. Furthermore, we present a reaction pathway for the synthesis of a class of seven T_MB intermetallics, containing transition metals V, Nb, Ta, Cr, Mo, W, and Ru, and experimentally identify RuB as an efficient hydrogen-evolving catalyst for the HER. Despite recent studies on the hydrogen-evolution catalytic activity of MoB,[10] the catalytic

[*] X. Ai,[+] X. Zou,[+] Dr. H. Chen,[+] Q. Li, Dr. Y. Liu, Prof. X. Zou
State Key Laboratory of Inorganic Synthesis and Preparative Chemistry, College of Chemistry, Jilin University
Changchun 130012 (P. R. China)
E-mail: xxzou@jlu.edu.cn
Y. Su, X. Feng, Prof. Y. Zhang
Key Laboratory of Bio-Inspired Smart Interfacial Science and Technology of Ministry of Education, School of Chemistry and Environment, Beihang University
Beijing 100191 (P. R. China)
[+] These authors contributed equally to this work.
Supporting information and the ORCID identification number(s) for the author(s) of this article can be found under: https://doi.org/10.1002/anie.201915663.

abilities for HER of other T_MB intermetallics have never been revealed both theoretically and experimentally.

We compared fifteen pure transition metals (T_M) with their corresponding T_MB intermetallics for investigating the regulating effect of boron atoms on surface hydrogen adsorption property (see details in the Theoretical Section in the Supporting Information and Tables S1–S7 and Figures S1, S2). The chemisorption of hydrogen atom on the surface is the key element reaction of some catalysis processes, such as electrocatalytic hydrogen evolution, hydrodesulfurization, and nitrogen fixation.[11] According to packing patterns of metal atoms, the fifteen transition metals can be classified into two types, including the body-centered-cubic structure (T_M = V, Nb, Ta, Cr, Mo, and W) and the closest packed structure (T_M = Rh, Ir, Pd, Ni, Ti, Zr, Ru, Os, and Re), as shown in the Supporting Information, Figure S1. While the T_MB can maintain the similar packing structures of metal atoms to their parent metals, the presence of interstitial B atoms leads to an expansion of crystal lattices to some extent. For example, Ru atoms in RuB maintain the hexagonal packed structure of metallic Ru (Figure 1 a,b), and Ta atoms in TaB preserve the body-centered-cubic structure of metallic Ta (Figure 1 c,d).

We conduct density functional theory (DFT) calculations to investigate stable hydrogen adsorption sites on close-packed surfaces of these transition metals and their corresponding T_MB intermetallics (Supporting Information, Figures S1, S2). The results (Supporting Information, Tables S2, S3) show that the most favorable hydrogen adsorption sites are the three-fold hollow sites for transition metals, except that the top site is the most favorable one for iridium. As shown in the Supporting Information, Tables S4–S6, the T_MB intermetallics based on Rh, Pd, Ti, Zr, Ru, and Re maintain the three-fold hollow site as the most favorable adsorption site, while other T_MB intermetallics transfer the most favorable adsorption site to bridge site (T_M = V, Nb, Ta, Cr, Mo, W, Ni) or top site (T_M = Os, Ir). Compared with pure metals (Figure 1 e), their corresponding T_MB intermetallics generally exhibit weaker hydrogen adsorption on their surfaces.

This modulation of the surface adsorption properties can affect the catalytic activity of T_MB intermetallics for the HER, which is of technological importance in some applications (for example, water electrolysis, chlor-alkali electrolysis).[11] To evaluate the catalytic activity, the adsorption free energy of atomic hydrogen (ΔG_{H^*}) on T_MB intermetallic surfaces are calculated. An optimum hydrogen-evolving catalyst (that is, the benchmark catalyst Pt) should hold a near-zero ΔG_{H^*} value at its catalytic site. Figure 1 f and the Supporting Information, Table S7 present the ΔG_{H^*} values on metal-terminated surfaces of these T_MB intermetallics. For comparative purposes, the ΔG_{H^*} value of Pt (111) surface (the model surface of Pt) is also included. The result reveals that several T_MB intermetallics (PdB, RuB, and ReB) exhibit appropriate ΔG_{H^*} values and thereby should have efficient catalytic activity for HER.

To reveal the roles of boron atom in weakening of the hydrogen adsorption energy at metal site, we conducted a comparative study on the electronic structures of pure transition metals and the corresponding T_MB intermetallic, taking Ru and RuB for example. Figure 2 a shows the density of states (DOS) and projected density of states (pDOS) of Ru and RuB. The Fermi levels of Ru and RuB are both crossed by the DOS, suggesting that RuB is conductive and has metallic property similar to metallic Ru. Furthermore, the d-band of Ru atom is the major contribution to the total states for metallic Ru and RuB. Compared with metallic Ru, the d-band center (a key characteristic of the electronic structure) of RuB downshifts away from Fermi level (Supporting Information, Table S8), and correspondingly, the antibonding state decreases in energy and becomes more occupied. This will lead to a weaker H adsorption and optimal ΔG_{H^*} value, according to the d-band theory.[12]

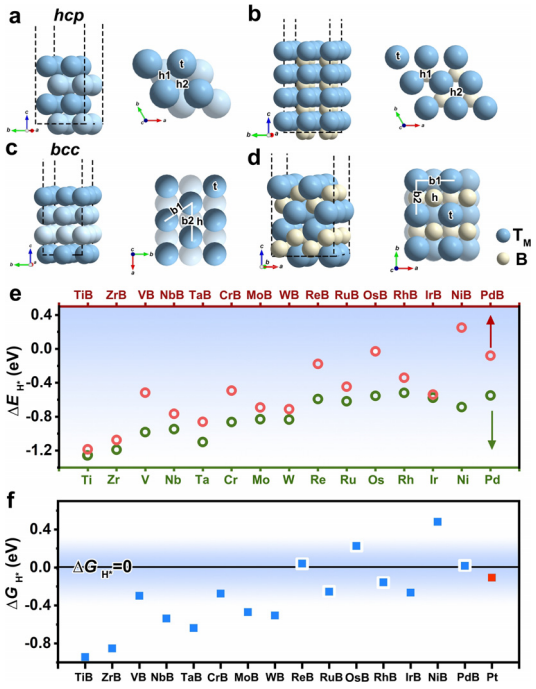

Figure 1. The atomic arrangement models of a),c) transition metals and b),d) their corresponding T_MB intermetallics. e) Calculated ΔE_{H^*} values of fifteen pure transition metals and corresponding T_MB intermetallics. f) Calculated ΔG_{H^*} values of fifteen T_MB intermetallics and Pt.

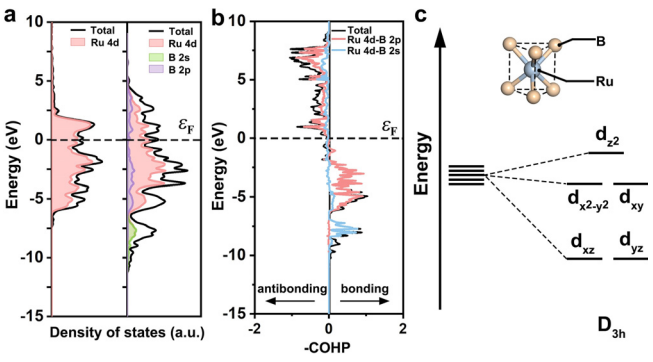

Figure 2. a) Calculated DOS and pDOS of Ru (0001) surface and RuB (001) surface. b) COHP of the Ru–B bond in RuB. c) The occupation of electrons in Ru 4d orbitals under the crystal field of RuB.

We further investigated some important factors responsible for the modification of Ru d-band properties. We first examine whether the incorporation of B atoms in metallic Ru framework changes the filling of the surface d-band. The result (Supporting Information, Table S8) shows that the change in d-band filling between Ru and RuB is less than 5%. Furthermore, Bader charge analysis shows that only 0.01 electrons (|e|) transfer from the Ru atom to the B atom in RuB. Thus, the slight changes in the filling of the d-band and the charge transfer are unlikely to be the reasons for the modified d-band property of RuB.

We next examine the strain and the ligand effects on the d-band properties. On the one hand, the incorporation of B atoms in metallic Ru framework leads to the expansion of the crystal lattice. This tensile strain will reduce the Ru d-orbital overlap and thereby result in a narrowing of the d-band and an upshift of d-band center (that is, the strain effect). On the other hand, the orbital hybridization between Ru and B atoms will cause the broadening of d-band and downshift of d-band center (that is, the ligand effect). The orbital hybridization between Ru and B atoms in RuB can be reflected by its pDOS and the crystal orbital Hamiltonian population (COHP) for the Ru–B bond. As shown in Figure 2a,b, there are the DOS overlap and the bonding between of Ru d orbital and B sp orbitals in RuB. The above analysis suggests that the ligand effect should be dominate to the strain effect, and their integrative effects finally generate the downshift of d-band center in RuB.

To further understand why orbital hybridization between Ru and B atoms causes a downshift of d-band center (or a broadening of d-band) in RuB, we investigate the coordination environment of Ru atoms in the framework of crystal field theory. As shown in Figure 2c (inset), Ru atom and its six neighboring B atoms form an octahedral field with D_{3h} symmetry.[13] As shown in Figure 2c and the Supporting Information, Table S9, the five 4d orbitals of Ru atom in the octahedral field of six surrounding boron atoms split into three orbital groups (that is, d_{z^2}, $d_{xz,yz}$, $d_{x^2-y^2,xy}$). The $d_{xz,yz}$ orbitals are double-degenerate and are the lowest in energy due to their strong hybridization with the sp orbitals of B atom. The $d_{x^2-y^2,xy}$ orbitals are also degenerate, with a moderate energy. Compared with $d_{x^2-y^2,xy}$ and $d_{xz,yz}$ orbitals, the d_{z^2} orbital has a weak hybridization with B atoms owing to the mismatching orbital symmetry. The above results, coupled with the fact that the five 4d orbitals of Ru atom in metallic Ru are degenerate in energy, the strong hybridization of Ru $d_{xz,yz}$ orbitals and sp orbitals of B atom is the fundamental cause of the modified d-band properties in RuB.

These theoretical results inspire us to synthesize a class of T_MB intermetallics and to investigate their electrocatalytic activities for HER. Traditionally, the synthesis of T_MB intermetallics was based on the chemical reaction between element metal (T_M) and boron (B), $T_M + B = T_MB$ (Route I in Figure 3a). This synthetic route required harsh experimental conditions (such as high temperature and high pressure), and often gave the target products with some residual boron impurities or other undesirable boride phases.[9,14] Here, we propose a general synthetic route for the synthesis of phase-pure T_MB intermetallics. This synthetic route is based on the

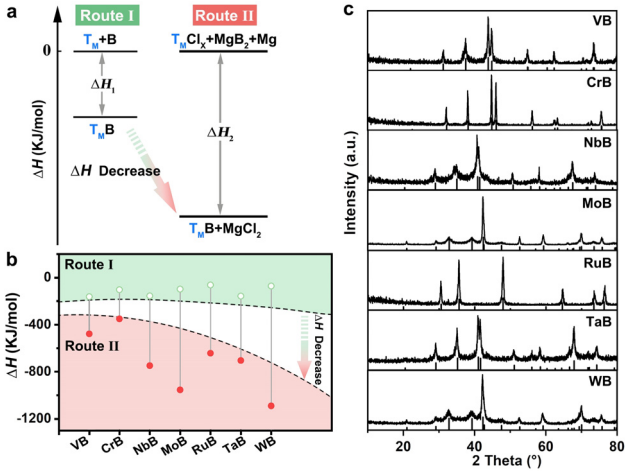

Figure 3. a) The reaction routes for the synthesis of T_MB intermetallics and b) calculated reaction enthalpies of traditional element reaction (Route I) and magnesiothermic reduction in this work (Route II). c) The XRD patterns of T_MB intermetallics. For comparison, the standard XRD cards of these T_MB intermetallics are included in (c).

magnesiothermic reduction reaction under relatively mild conditions, $T_MCl_x + Mg + MgB_2 \rightarrow MgCl_2 + T_MB$ (Route II in Figure 3a), followed by the removal of the by-product, $MgCl_2$ (see details in the Experimental Section in the Supporting Information and Table S10). By using this reaction pathway, seven phase-pure T_M intermetallics, including VB, NbB, TaB, CrB, MoB, WB, and RuB, are synthesized. As shown in Figure 3b and the Supporting Information, Tables S11, S12, the reaction enthalpy changes (ΔH) of Route I and Route II are compared. The result shows that the Route II has a significantly more negative ΔH in comparison to that of the Route I, suggesting that the Route II is more thermodynamically favorable reaction pathway for accessing T_M intermetallics.

As shown in Figure 3c, the powder X-ray diffraction (XRD) results reveal that the as-synthesized seven samples are phase-pure T_MB intermetallics, including VB, NbB, TaB, CrB, MoB, WB, and RuB. Transmission electron microscopy (TEM) images show that MoB, WB, TaB, VB, NbB, and RuB are composed of nanoparticles of around 20–150 nm, with the exception of CrB consisting of particles of around 2 μm (Supporting Information, Figure S3). Furthermore, the Brunauer–Emmett–Teller (BET) specific surface areas for these T_MB intermetallics are in the range of 3–50 $m^2 g^{-1}$ (Supporting Information, Table S13). These results suggest that the magnesiothermic reduction reaction (Route II) is an effective route for the synthesis of phase-pure T_MB intermetallics.

Next, we studied the electrochemical activities of the seven T_MB intermetallics toward HER in 0.5 M H_2SO_4 solution (see details in Experimental Section of the Supporting Information). Figure 4a shows the overpotentials required to reach the current density of 10 mA cm^{-2} (normalized by the geometric surface area of the electrode). While RuB needs the smallest overpotential to reach 10 mA cm^{-2} current density (that is, the best catalytic activity) among these seven T_MB intermetallics, WB exhibits the highest catalytic activity among non-precious intermetallic

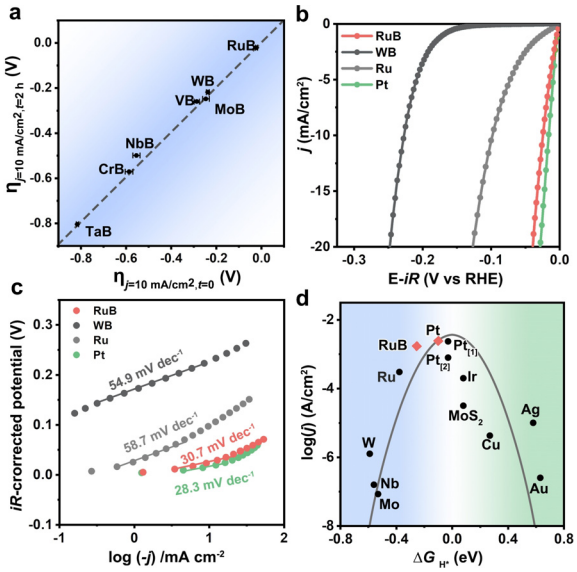

Figure 4. a) The electrocatalytic activity and short-term stability of seven T_MB intermetallics toward HER in acidic solution. The *x*-axis and *y*-axis represent the overpotentials required to reach the current density of 10 mA cm^{-2} at times $t = 0$ h and $t = 2$ h. The dashed line is the ideal response of a stable catalyst. b) Polarization curves of RuB, WB, Ru, and Pt in acidic solution with 85% *iR* compensation. c) Tafel plots for HER over RuB, WB, Ru, and Pt. d) A volcano plot showing the exchange current densities for HER as a function of calculated ΔG_{H^*} values for different materials. The data for a variety of metals and MoS_2 are taken from Ref. [15]. The data for Pt[1] and Pt[2] are taken from Refs. [15a] and [16].

T_MB. Moreover, these seven T_MB catalysts have no obvious activity loss after the HER for two hours at 10 mA cm^{-2} current density (Figure 4a), suggesting their good stabilities in catalyzing HER.

For comparative purpose, we also synthesized metallic Ru and Pt nanoparticles (Supporting Information, Figures S4, S5), and evaluated their catalytic activities under the same conditions. Figure 4b and the Supporting Information, Figure S6 show the polarization curves of seven T_MB intermetallics, Pt and Ru for HER in acidic solution. RuB exhibits a remarkable catalytic activity toward HER, which is close to that of Pt and much better than that of metallic Ru. In particular, RuB requires an overpotential of 22 mV at 10 mA cm^{-2} current density, and WB exhibits a good catalytic activity, achieving 10 mA cm^{-2} at an overpotential of 228 mV. The specific activities of seven T_MB intermetallics and Pt are further compared by normalizing the measured currents with respect to BET surface areas (Supporting Information, Figure S7). The results reveal that RuB maintains the highest HER catalytic activity among the seven T_MB intermetallics and has Pt-like activity. We note that the catalytic activity of RuB is also comparable to that of commercial 20 wt% Pt/C catalyst (Supporting Information, Figure S8a,b). Furthermore, RuB displays a good catalytic stability (Supporting Information, Figures S8c) and structural stability (Supporting Information, Figures S9) for at least ten hours and nearly 100% faradaic efficiency during HER (Supporting Information, Figure S8d), indicating that the observed current passed through the catalyst is exclusively used for catalyzing the HER.

We further compared the Tafel slopes of Pt, Ru, RuB, and WB in Figure 4c. RuB has a Tafel slope of 30.7 mV dec^{-1}, close to that of Pt (28.3 mV dec^{-1}) and much smaller than that of Ru (58.7 mV dec^{-1}). And WB has a Tafel slope of 54.9 mV dec^{-1}. These results suggest that the HER kinetic for RuB and WB should follow the Volmer–Tafel mechanism and the Volmer–Heyrovsky mechanism, respectively.[17] The apparent exchange current density versus ΔG_{H^*} for RuB (2.493 mA cm^{-2}) as well as several representative metals and MoS_2, the values of which were taken from previous reports for comparative purposes, is plotted in Figure 4d. RuB is seen to be around the top of the volcano curve, and its apparent exchange current density is a little smaller than that (3.421 mA cm^{-2}) of the Pt catalyst. This result further demonstrates that RuB is a highly active material for catalyzing the HER.

In summary, we have demonstrated the nature of metal–boron orbital interactions as well as its influence on the surface adsorption property and catalytic activity in boron-bearing intermetallics. Several T_MB intermetallics (for example, PdB, RuB, and ReB) are predicted theoretically to possess platinum-like hydrogen-evolving catalytic activity. Additionally, a magnesiothermic reduction route is developed for the synthesis of a class of seven phase-pure T_MB intermetallics that are not readily available traditionally. Furthermore, RuB is identified experimentally as an efficient material with catalytic activity approaching that of platinum for HER. Our results presented here could encourage further research of boron-containing intermetallics as prospective catalysts for various useful chemical reactions, beyond the HER.

Acknowledgements

Xi.Z. acknowledges the financial support from the National Natural Science Foundation of China (NSFC) Grant No. 21771079 and 21922507, Program for JLU Science and Technology Innovative Research Team (JLUSTIRT) and Fok Ying Tung Education Foundation, Grant No. 161011. Y. Zhang thanks NSFC Grant No. 51925202 and 21771013 for financial support. H.C. acknowledges the financial support from NSFC Grant No. 21901083, Postdoctoral Innovative Talent Support Program Grant No. BX20180120 and China Postdoctoral Science Foundation Grant No. 2018M641771. We also thank NSFC (21621001) and the 111 Project (B17020) for financial support.

Conflict of interest

The authors declare no conflict of interest.

Keywords: active sites · boron · electrocatalysis · electronic structure · intermetallic compounds

How to cite: *Angew. Chem. Int. Ed.* **2020**, *59*, 3961 – 3965
Angew. Chem. **2020**, *132*, 3989 – 3993

[1] A. J. Medford, A. Vojvodic, J. S. Hummelshøj, J. Voss, F. A. Pedersen, F. Studt, T. Bligaard, A. Nilsson, J. K. Nørskov, *J. Catal.* **2015**, *328*, 36 – 42.
[2] a) M. Wang, B. Wang, F. Huang, Z. Lin, *Angew. Chem. Int. Ed.* **2019**, *58*, 7526 – 7536; *Angew. Chem.* **2019**, *131*, 7606 – 7616; b) R. Li, E. F. Antunes, E. Kalfon-Cohen, A. Kudo, L. Acauan, W.-C. D. Yang, C. Wang, K. Cui, A. H. Liotta, A. G. Rajan, J. Gardener, D. C. Bell, M. S. Strano, J. A. Liddle, R. Sharma, B. L. Wardle, *Angew. Chem. Int. Ed.* **2019**, *58*, 9204 – 9209; *Angew. Chem.* **2019**, *131*, 9302 – 9307; c) T. Choksi, P. Majumdar, J. P. Greeley, *Angew. Chem. Int. Ed.* **2018**, *57*, 15410 – 15414; *Angew. Chem.* **2018**, *130*, 15636 – 15640.
[3] a) M. Luo, Z. Zhao, Y. Zhang, Y. Sun, Y. Xing, F. Lv, Y. Yang, X. Zhang, S. Hwang, Y. Qin, J.-Y. Ma, F. Lin, D. Su, G. Lu, S. Guo, *Nature* **2019**, *574*, 81 – 85; b) H. Chen, X. Ai, W. Liu, Z. Xie, W. Feng, W. Chen, X. Zou, *Angew. Chem. Int. Ed.* **2019**, *58*, 11409 – 11413; *Angew. Chem.* **2019**, *131*, 11531 – 11535; c) E. Peiris, S. Sarina, E. R. Waclawik, G. A. Ayoko, P. Han, J. Jia, H.-Y. Zhu, *Angew. Chem. Int. Ed.* **2019**, *58*, 12032 – 12036; *Angew. Chem.* **2019**, *131*, 12160 – 12164; d) M. G. Vinum, M. R. Almind, J. S. Engbæk, S. B. Vendelbo, M. F. Hansen, C. Frandsen, J. Bendix, P. M. Mortensen, *Angew. Chem. Int. Ed.* **2018**, *57*, 10569 – 10573; *Angew. Chem.* **2018**, *130*, 10729 – 10733; e) L. Lu, X. Sun, J. Ma, D. Yang, H. Wu, B. Zhang, J. Zhang, B. Han, *Angew. Chem. Int. Ed.* **2018**, *57*, 14149 – 14153; *Angew. Chem.* **2018**, *130*, 14345 – 14349.
[4] L. Rößner, M. Armbrüster, *ACS Catal.* **2019**, *9*, 2018 – 2062.
[5] a) B. Hammer, J. K. Nørskov, *Surf. Sci.* **1995**, *343*, 211 – 220; b) A. Ruban, B. Hammer, P. Stoltze, H. L. Skriver, J. K. Nørskov, *J. Mol. Catal. A Chem.* **1997**, *115*, 421 – 429.
[6] a) Y. Zheng, Y. Jiao, M. Jaroniec, S. Z. Qiao, *Angew. Chem. Int. Ed.* **2015**, *54*, 52 – 65; *Angew. Chem.* **2015**, *127*, 52 – 66; b) Z. Chen, Y. Song, J. Cai, X. Zheng, D. Han, Y. Wu, Y. Zang, S. Niu, Y. Liu, J. Zhu, X. Liu, G. Wang, *Angew. Chem. Int. Ed.* **2018**, *57*, 5076 – 5080; *Angew. Chem.* **2018**, *130*, 5170 – 5174; c) Q. Li, X. Zou, X. Ai, H. Chen, L. Sun, X. Zou, *Adv. Energy Mater.* **2019**, *9*, 1803369.
[7] a) T. Chao, X. Luo, W. Chen, B. Jiang, J. Ge, Y. Lin, G. Wu, X. Wang, Y. Hu, Z. Zhuang, Y. Wu, X. Hong, Y. Li, *Angew. Chem. Int. Ed.* **2017**, *56*, 16047 – 16051; *Angew. Chem.* **2017**, *129*, 16263 – 16267; b) X. Lu, Y. Wu, X. Yuan, H. Wang, *Angew. Chem. Int. Ed.* **2019**, *58*, 4031 – 4035; *Angew. Chem.* **2019**, *131*, 4071 – 4075; c) C. Wang, H. Yang, Y. Zhang, Q. Wang, *Angew. Chem. Int. Ed.* **2019**, *58*, 6099 – 6103; *Angew. Chem.* **2019**, *131*, 6160 – 6164.
[8] J. Nagamatsu, N. Nakagawa, T. Muranaka, Y. Zenitani, J. Akimitsu, *Nature* **2001**, *410*, 63 – 64.
[9] G. Akopov, M. T. Yeung, R. B. Kaner, *Adv. Mater.* **2017**, *29*, 1604506.
[10] a) Y. Chen, G. Yu, W. Chen, Y. Liu, G.-D. Li, P. Zhu, Q. Tao, Q. Li, J. Liu, X. Shen, H. Li, X. Huang, D. Wang, T. Asefa, X. Zou, *J. Am. Chem. Soc.* **2017**, *139*, 12370 – 12373; b) H. Vrubel, X. Hu, *Angew. Chem. Int. Ed.* **2012**, *51*, 12703 – 12706; *Angew. Chem.* **2012**, *124*, 12875 – 12878; c) H. Park, A. Encinas, J. P. Scheifers, Y. Zhang, B. P. T. Fokwa, *Angew. Chem. Int. Ed.* **2017**, *56*, 5575 – 5578; *Angew. Chem.* **2017**, *129*, 5667 – 5670; d) Z. Zhuang, Y. Li, Z. Li, F. Lv, Z. Lang, K. Zhao, L. Zhou, L. Moskaleva, S. Guo, L. Mai, *Angew. Chem. Int. Ed.* **2018**, *57*, 496 – 500; *Angew. Chem.* **2018**, *130*, 505 – 509.
[11] a) J. G. Chen, R. M. Crooks, L. C. Seefeldt, K. L. Bren, R. M. Bullock, M. Y. Darensbourg, P. L. Holland, B. Hoffman, M. J. Janik, A. K. Jones, M. G. Kanatzidis, P. King, K. M. Lancaster, S. V. Lymar, P. Pfromm, W. F. Schneider, R. R. Schrock, *Science* **2018**, *360*, eaar6611; b) X. Zou, Y. Zhang, *Chem. Soc. Rev.* **2015**, *44*, 5148 – 5180.
[12] J. K. Nørskov, F. Studt, F. Abild-Pedersen, T. Bligaard, *Fundamental Concepts in Heterogeneous Catalysis*, Wiley, Hoboken, **2014**.
[13] R. Krishnamurthy, W. B. Schaap, *J. Chem. Educ.* **1969**, *46*, 799.
[14] a) N. N. Greenwood, R. V. Parish, P. Thornton, *Q. Rev. Chem. Soc.* **1966**, *20*, 441 – 464; b) L. Han, S. Wang, J. Zhu, S. Han, W. Li, B. Chen, X. Wang, X. Yu, B. Liu, R. Zhang, Y. Long, J. Cheng, J. Zhang, Y. Zhao, C. Jin, *Appl. Phys. Lett.* **2015**, *106*, 221902.
[15] a) J. K. Nørskov, T. Bligaard, A. Logadottir, J. R. Kitchin, J. G. Chen, S. Pandelov, U. Stimming, *J. Electrochem. Soc.* **2005**, *152*, J23 – J26; b) B. Hinnemann, P. G. Moses, J. Bonde, K. P. Jørgensen, J. H. Nielsen, S. Horch, I. Chorkendorff, J. K. Nørskov, *J. Am. Chem. Soc.* **2005**, *127*, 5308 – 5309.
[16] S. Trasatti, *J. Electroanal. Chem.* **1972**, *39*, 163 – 184.
[17] J. O. Bockris, E. C. Potter, *J. Electrochem. Soc.* **1952**, *99*, 169 – 186.

Manuscript received: December 8, 2019
Accepted manuscript online: January 3, 2020
Version of record online: January 30, 2020

